Global and local fatigue analysis of X100 and X60 steel catenary riser girth welds

Ronan J. Devaney*[1,3], Padraic E. O'Donoghue[2,3], Sean B. Leen[1,3]

[1]*Department of Mechanical Engineering, College of Engineering & Informatics, National University of Ireland, Galway, Ireland.*

[2]*Department of Civil Engineering, College of Engineering & Informatics, National University of Ireland, Galway, Ireland.*

[3]*Ryan Institute for Environmental, Marine and Energy Research, National University of Ireland, Galway, Ireland.*

*r.devaney1@nuigalway.ie – 00353862483179

Acknowledgements

This publication has emanated from research conducted with the financial support of Science Foundation Ireland as part of the MECHANNICS joint project between NUI Galway and University of Limerick under Grant Number SFI/14/IA/2604.

The authors would also like to thank Dr. Adrian Connaire of Wood Group Kenny for his advice and support in providing the Flexcom software used in this publication.

Stress analysis of welded steel catenary risers

The use of steel catenary risers in offshore oil and gas production has increased significantly in recent years due to some distinct advantages over flexible risers, in particular for deepwater applications. The motivation for this paper is to develop a detailed assessment approach with respect to welded steel catenary risers, thus reducing the requirement for overly conservative factors of safety. This paper presents a global-local finite element modelling approach, with the Flexcom offshore dynamic analysis package used to determine the global load quantities for two ultra-deepwater free hanging steel catenary risers. These results then act as stress boundary conditions in a local model created using Abaqus, with the analysis focusing on the failure susceptible regions such as in the vicinity of a girth weld. The methodology accounts for the geometrical discontinuities of the weld and the different mechanical properties of the parent material, weld metal and heat affected zone, which result in fatigue hotspots for dynamic structures such as steel catenary risers.

Material properties for two line pipe steels, a current generation X60 and a next generation X100 are investigated in the local analysis. Two pipe wall thicknesses are examined, with the weld geometry being different for each and it is shown that this weld detail can lead to significantly different stress concentrations. X100 is shown to be superior to X60 with respect to yielding and fatigue for both geometries.

Keywords: Weld; Steel catenary riser; Fatigue; Energy; Structure; Offshore

Introduction

According to recent statistics published by the US energy information administration (Manning, 2016), global deepwater (125 m to 1,500 m deep) oil production has increased by 25% and ultra-deepwater production (deeper than 1500 m) has risen by over 500% in the past decade amidst stagnant total offshore production levels. Steel catenary risers (SCRs) have become established as a capable and cost effective pipeline technology in deepwater and ultra-deepwater locations due to their advantages in addressing the key challenges of deepwater riser design, namely, collapse capacity,

weight limitations, corrosion and temperature resistance. This has resulted in a significant number of recent installations in cutting-edge deepwater projects and high levels of specification for future developments.

Fatigue performance is one of the primary design challenges for SCRs as highlighted by Abelanet et al (Abelanet, Karunakaran, Jones, Eyssautier, & White, 2013), which are subjected to extreme dynamic loading due to ocean wave motion and the associated excitation caused by floating production facilities, vortex induced vibrations and cyclic pressurisation. As a result of this highly complex and unpredictable loading environment, SCR components are often specified with a fatigue factor of safety of 10 in order to avert catastrophes such as the recent Deepwater Horizon accident, which is estimated to have cost BP a total of $61.6 billion as well as causing untold damage to natural habitats along the Gulf of Mexico (GoM) coast, well documented in a review by Beyer and co-workers (Beyer, Trannum, Bakke, Hodson, & Collier, 2016).

Welded connections have long been recognised as a primary source of fatigue failures for offshore structures in the petroleum industry as highlighted by Wirsching (Wirsching, 1984). More recently detailed work has been conducted on creep-fatigue (CF) failure in the welded connections of steam headers in power plants under flexible operation. Farragher and co-workers (Farragher, Scully, O'Dowd, Hyde, & Leen, 2014) characterised the constitutive behaviour of the parent material (PM), weld metal (WM) and heat affected zone (HAZ) of a P91 joint, by individually identifying the PM and WM parameters experimentally and then iteratively identifying the HAZ parameters through finite element (FE) modelling and comparison with cross-weld (CW) experimental data. Following on from this work, Li et al. (Li et al., 2016) used an in series spring model to identify the elastic modulus of the P91 HAZ and the results of

hardness tests to identify the yield stress, before identifying the remaining plasticity parameters through FE modelling and comparison with CW experimental data. The identified constitutive parameters were then applied to a detailed steam header T-joint FE model to successfully predict the location of (CF) failure hot spots.

However, relatively little detailed analysis of fatigue and plasticity in such detail has been applied to the specific case of fatigue in SCR fatigue welded connections. The welded connections of SCRs are particularly susceptible to fatigue failure, due to the combined effect of the geometrical discontinuity, material mismatch and the potential defects from the welding process such as misalignment, lack of fusion or penetration according to Kopp and co-workers (Kopp, Perkins, Prentice, & Stevens, 2003). Clearly, in order to safely and efficiently design next generation SCR systems, a greater understanding of the loading conditions and constitutive material behaviour at the welded connections is required.

Global-local modelling is an invaluable technique for detailed analysis of a region of interest on a large dynamic structure. This technique has previously been applied to SCRs by Hu and co-workers (Hu, Campbell, & Huang, 2014) to model in detail the seabed-riser interaction at the touchdown zone. A further advantage of global-local modelling is the potential for the application of complex fatigue failure criteria, such as that developed by Lemaitre et al (Lemaitre & Desmorat, 2005), to a local region of interest on a large structure such as an SCR.

In the present work, the Flexcom offshore dynamic structural analysis FE software package is used to predict the global response for two free hanging SCR models, both connected to a floating production, storage and offloading facility (FPSO) at a wide range of wave amplitudes. Two detailed local girth weld FE models, representative of a girth weld for each of the global SCR models, are also created in the

general purpose FE solver Abaqus. The detailed local girth weld models incorporate a weld geometry based on those reported by Mecozzi et al. in the FATHOMS report (Mecozzi et al., 2010), with separate material properties applied to the PM, WM and HAZ for two high strength low alloy (HSLA) steels, X60 and X100. The loading applied to the local model is obtained from the critical failure zone of the SCR models determined during the global analysis using Flexcom. This global-local modelling methodology allows for accurate and efficient assessment of the resulting stress-strain history at a welded joint of a large scale SCR system due to in-service conditions.

The motivation for this research is to develop a detailed assessment approach with respect to SCR welds, thus reducing the requirement for overly-conservative factors of safety. By implementing a more efficient analysis and design methodology for SCRs, it will be possible to further exploit the weight reduction and increased capacity facilitated by the development of next generation high HSLA steels such as X100.

The resulting SCR weight reductions have the potential to deliver significant cost savings in offshore projects, by minimising the buoyant support required from floating production facilities and increasing pipe laying productivity. This improvement in the SCR design capability will allow for economically viable access to new ultra-deepwater (deeper than 1,500 m) resources by enabling the use of more conventional and cost effective riser technologies.

Modelling

Global riser model

The global dynamic analyses is conducted on two SCR models using the Flexcom offshore dynamic structural analysis FE software package, developed by Wood Group

Kenny (*Flexcom Version 8.4.1 Software Documentation*, 2015).

Two global SCR configurations were analysed and both consist of a FPSO from which a free hanging SCR with a total length of 4298.5 m is suspended, with its end lying on the seabed at a depth of 3000 m as shown in Figure 1. This sea depth is chosen as being representative of the current frontier in ultra-deepwater offshore oil and gas production according to Saglar and co-workers (Saglar, Toleman, & Thethi, 2015). For example, Shell's Perdido in the GoM is currently the world's deepest fully operational production platform at a depth of 2,450 m. Initial production began in September 2016 at the Shell stones field, also in the GoM at a depth of 2,926 m, which is expected to be fully operational by the end of 2017. At the Stones field a form of SCR technology known as a steel lazy wave riser is used, where the riser has sections of additional buoyancy added mid length, resulting in the formation of an arched bend in the riser between the seabed and waterline. This bend in the SCR acts to partially absorb the motion of the FPSO, reducing the loading at critical locations on the riser. The risers are connected to a FSPO via the world's largest buoyant turret mooring in order to allow the FPSO to disconnect during extreme weather events.

In the global dynamic analysis conducted as part of this work, the SCR is connected to the FSPO by means of a flex joint and an I-tube, while the seabed end of the SCR is fixed in position. The SCRs are modelled as plain pipes without weld profiles, with an outer diameter of 406.4 mm during the global analysis. Two different wall thicknesses (WT) 15 mm and 25 mm are considered in order to investigate the effect of wall thickness. The elastic material properties and riser dimensions used for both global SCR models are shown in Table 1.

During global analysis in Flexcom the SCRs are modelled using two-noded hybrid beam-column elements with 14 degrees of freedom, which were developed by

O'Brien et al. (O'Brien, McNamara, & Grealish, 1991) and are specifically designed to accommodate the low bending stiffness and arbitrarily large 3D non-linear displacements and rotations of flexible risers. For element refinement purposes the global SCR models are subdivided into three zones, the seabed zone (550 m), the touchdown zone (200 m) and the riser column (3,548.5 m) as shown in Figure 1. A total of 705 elements are used in each of the global SCR models. Refined 1.5 m elements are used to capture the high gradients in loading at the touchdown zone, while the element size is varied between 1.5 m and 7.5 m in the seabed zone and riser column.

For both SCR configurations the flex joint is modelled as a linear 0.5 m beam element with a mass of 102 kg and a rotational stiffness of 21.63 kN.m/degree, and the final element connecting the SCR to the FPSO is modelled as a rigid I-tube of length 1 m.

The SCR-seabed interaction is modelled as a beam on elastic foundation, with a stiffness of 143.4 kN/m/m. Standard seabed properties obtained from the Flexcom examples manual (*Flexcom Version 8.4.1 Examples Manual*, 2015) are assigned, with friction coefficients of 0.2 and 0.4 and friction stiffnesses of 45 N/m/m and 90 N/m/m assigned in the longitudinal and transverse directions respectively. The flex joint and I-tube properties used during analysis were obtained from the Flexcom examples manual (*Flexcom Version 8.4.1 Examples Manual*, 2015). During all analyses the SCR is modelled as containing crude oil with a density of 870 kg/m^3 at a mean waterline pressure of 18 MPa, while the seawater density is assumed to be 1025 kg/m^3.

The dynamic global analyses are conducted for both SCR models using regular Airy waves, at wave amplitudes ranging from 1 m to 10 m. This wide range of wave amplitudes analysed corresponds to a variety of loading conditions, from everyday wave loading to 1000 year storms at offshore production zones throughout the globe. A

piecewise linear time independent current model is specified in all analyses. A velocity of 0.3 m/s is specified from the waterline to a sea depth of 55 m, which then decreases linearly to 0.15 m/s at a depth of 100 m and remains constant to the seabed.

Local girth weld model

The detailed local girth weld models created in Abaqus are based on an axisymmetric geometry and loading assumption, including only the axial stress and pressure loading components. The loading on the SCR due to bending is not accounted for explicitly in the local modelling of the girth weld, the justification for this is addressed below in the discussion section.

The output of the global SCR model analyses acts as an input to the local girth weld model by providing the boundary conditions for the combined axial stress, internal pressure and external pressure loading. The loading applied to the local girth weld model is taken from the critical failure location determined during global analysis. The axial stress at this location is applied to the local girth weld model as a uniform pressure acting in the longitudinal direction across the wall at one end, while the model is axially constrained at the opposite end. The internal pressure obtained from the global analysis is applied along the inner surface of the local girth weld model, while the hydrostatic pressure at this location is applied over the outer surface.

The local analyses are conducted using material properties representative of two HSLA line pipe steels, X60 and X100 (API Specification 5L & ISO 3183, 2008). The elastic-perfectly plastic material model is used in all cases, with separate material properties assigned to the three constituent weldment zones, PM, WM and HAZ, as labelled in Figure 2. The material properties used during analysis of the local girth weld model are shown in Table 2. The X60 material properties used were experimentally determined by Netto et al (Netto, Botto, & Lourenco, 2008). The X100 material

properties used for the PM and the WM are based on those measured by Ishikawa and co-workers (Ishikawa et al., 2008), while the X100 HAZ material properties have been estimated based on the common observation of a reduced yield stress in the HAZ in comparison with the parent material, as observed for the X60 material.

CAX8R axisymmetric eight node reduced integration quadratic elements are used for the local girth weld models. A suitable mesh for each of the local girth weld models was confirmed through mesh convergence studies with respect to the maximum axial stress predicted at a 2 m wave amplitude using X60 material properties. The results of the mesh convergence study are shown in Figure 3. Convergence was achieved using a mesh of 7,747 elements on the 25 mm WT girth weld geometry and 16,740 elements on the 15 mm WT weld geometry. For each model the elements are biased towards the weld root, and the junctions of the PM, HAZ and WM as shown in Figure 4. The mesh is biased towards these regions to accurately capture stress concentrations and the effect of inhomogeneous material properties.

Results

Global analysis

The global dynamic analysis of the SCR models predicted that the critical failure location was in the hang-off zone of the SCR just below the FPSO, at a distance of 4,288 m along the SCR from the seabed end, as highlighted in Figure 5. This is an area of the riser well known for its susceptibility to fatigue failure as shown by Vicic-Perunovic and co-workers (Vidic-Perunovic, Guo, Wang, Hopen, & Head, 2014), and Chibueze et al. (Chibueze, Ossia, & Okoli, 2016). During the local girth weld analysis, it is assumed that the modelled girth weld is located in this critical failure location. This region experiences the highest levels of mean and alternating axial stress combined with

a local increase in the alternating and mean resultant bending moment.

The high mean axial stress in this location is due to the self-weight of the large SCR section which is suspended below. The heaving motion due to the waves and the associated excitation of the FPSO is the primary cause of the high alternating axial stress at this location as shown in Figure 6.

The peak bending moment at the hang-off zone shown in Figure 7, is a result of the discontinuity in stiffness at the transition between the SCR and the flex joint below the FPSO. The location of maximum mean and alternating bending moment is at the touch down zone of the SCR; it then dramatically reduces along the length of the SCR towards the FPSO, with a small sudden peak at the hang-off zone.

The combined effect of these loading modes on the SCR, in addition to the constant high levels of hoop stress near the FPSO as shown in Figure 6, result in the critical location being in the hang off zone for both global SCR models.

There is an approximately linear increase with wave amplitude, in the maximum axial stress predicted in the failure critical element of both the 15 mm and 25 mm WT SCR models, as shown in Figure 8. The 25 mm WT model predicts lower maximum axial stress levels in all cases.

The maximum resultant bending moment at the failure critical element increases significantly with wave amplitude as shown in Figure 9. The maximum resultant bending moment is greater in the 25 mm WT model for lower wave amplitudes due to its increased stiffness relative to the 15 mm WT model, but is exceeded by the maximum resultant bending moment on the 15 mm WT model at high wave amplitudes due to the increased excitation of the lighter riser section.

Local analysis

Figure 10 presents contour plots of the maximum axial stress distribution for the 25mm

WT model for both X60 and X100 at a 2 m wave amplitude. It has been established that yielding occurs on the inner surface of the riser, at the weld root in the HAZ for the X60 material, but yielding is not predicted at any of the analysed wave amplitudes for this model using X100 material properties. Thus, the X100 girth weld model is effectively elastic and an axial stress concentration factor (SCF) of 1.61 is predicted for the 25 mm WT model from the results based on the ratio of the peak axial stress in the HAZ at the weld root to the uniform axial stress away from the weld.

Contour plots of the maximum axial stress distribution for the 15 mm WT geometry at a 2 m wave amplitude are presented in Figure 11 for both the X60 and X100 materials. For both materials, HAZ yielding is predicted on the inner surface of the riser at the weld root, in the 15 mm WT model for all load cases analysed. To compare with the SCF for the 25 mm WT model, an additional analysis was conducted on the 15 mm WT model, at an applied lower axial stress such that yielding did not occur. A significant axial SCF of 4.48 was predicted at the HAZ in the weld root of the 15 mm WT model. This higher SCF is very much influenced by the detail of the weld root geometry (see Figure 2).

The critical location for the both of the local girth weld models is the weld root, at the junction of the WM and the HAZ. This form of SCR girth weld is heavily penalised in fatigue design codes as mentioned by Maddox et al. (Maddox, Speck, Razmjoo, & Park, 2008) due to the difficulty of ensuring a quality weld because of the lack of access to the weld root for inspection and control, and the unbacked welding technique which is typically used.

This highlights the importance of a qualified, consistent welding procedure for SCR girth welds. The level of control required to obtain a consistent root pass is considerably more difficult to attain for welding conducted on an offshore floating

facility. Reel-lay installation methods have an inherent advantage in this respect, by allowing for better control of the quality and consistency of the welds in the controlled environment of onshore welding workshop.

The effect of cyclic loading on the local girth weld models was examined by alternating the applied axial stress between the maximum and minimum values obtained during global analysis for a given wave amplitude. The hot spot location on the 25 mm WT model is located in the HAZ adjacent to the PM at the weld root as labelled point A in Figure 12 for X60, with yielding occurring in the HAZ in this case. The cyclic axial stress predicted at an 8 m wave amplitude this location using X60 material properties is shown in Figure 13. The maximum levels of axial stress and axial stress range occur within the first two loading cycles. During the subsequent cycles it can be seen that the maximum axial stress and axial stress range reduce to a constant level within 6 cycles due to stress redistribution and the elastic shakedown phenomenon.

Fatigue life estimation

The modified Goodman relation Eq. (1) is used to assess the allowable combinations of mean and alternating stress, such that a component can be expected to survive a given fatigue life which is determined by the fatigue limit of the material.

$$\sigma_a = \sigma_e \left(1 - \frac{\sigma_m}{\sigma_{TS}} \right) \tag{1}$$

where σ_a and σ_m are the stress amplitude and mean stress of loading respectively, σ_{TS} is the ultimate tensile strength, and σ_e is the fatigue limit for a given N_f. The Basquin equation for high-cycle fatigue (HCF) loading provides a relationship between stress

range at zero mean stress, $\Delta\sigma\big|_{\sigma_m=0}$, and number of cycles to failure, N_f , as shown in Eq. (2).

$$\Delta\sigma\big|_{\sigma_m=0} = \sigma_f^{'} N_f^{-b} \tag{2}$$

where $\sigma_f^{'}$ and b are material constants. The fatigue limit, σ_e, for a given total life, N_f , can be calculated as half of $\Delta\sigma\big|_{\sigma_m=0}$. Hence, by combining the Goodman curve with the Basquin equation, a Goodman-Basquin equation relating fatigue life to stress range and mean stress is formed Eq. (3) , as derived by Sweeney and co-workers (Sweeney, McHugh, McGarry, & Leen, 2012) for the fatigue analysis of cardiovascular stents:

$$N_f = \left[\frac{\Delta\sigma}{\sigma_f^{'}\left(1 - \frac{\sigma_m}{\sigma_{TS}}\right)} \right]^{\frac{1}{b}} \tag{3}$$

where $\Delta\sigma$ is the alternating stress range, $\sigma_f^{'}$ is the fatigue ductility coefficient and b is the fatigue strength exponent. The Goodman-Basquin relation is used in this work to estimate the fatigue life at the most highly stressed location in the PM, WM and HAZ for the 25 mm WT model at locations A, B and C as labelled in Figure 12. Although this relation is uniaxial, as the alternating and dominant mean stress for the local girth weld models are uniaxial, it has been deemed suitable for use for this preliminary study.

The material parameters for X60 and X100 used during the fatigue life calculations are shown in Table 2. The fatigue ductility coefficient and the fatigue strength exponent for each of the X60 and X100 weld zones were obtained by the universal slopes method, which allows for fatigue calculations based on the results of

uniaxial tensile test data, as outlined by Manson (Manson, 1965) and applied by Del Llano-Vizcaya et al. (Del Llano-Vizcaya, Rubio-González, Mesmacque, & Cervantes-Hernández, 2006) in the analysis of helical compression springs.

The X60 material properties used during the fatigue calculations were reported by Zhang et al. (Zhang & Dorn, 1998). The ultimate tensile strength of the PM was determined by means of a standard tensile test, while the ultimate tensile strength of the WM and HAZ were determined using the microshear test method. The X100 PM and WM ultimate tensile strength were measured by Ishikawa et al. (Ishikawa et al., 2008) using a standard tensile test, while the HAZ ultimate tensile strength was estimated from the results of hardness tests using a well-documented empirical relation Eq. (4) as described by Cahoon (Cahoon, 1972):

$$\sigma_{TS} = \frac{H}{3.1}\left(\frac{n}{0.217}\right)^{n} g \tag{4}$$

where H is Vickers hardness , n is the strain hardening coefficient and g is acceleration due to gravity.

The results shown in Figure 14 show the predicted results obtained using the combined Goodman-Basquin equation at locations A, B and C of the 25 mm WT model for both X60 and X100 materials at a range of wave amplitudes. The superior performance of the X100 material in this case study is clear from this preliminary analysis. Under normal operating conditions fatigue failure is not expected within the low-cycle fatigue (LCF) regime (less than 10^5 cycles) in any of the most highly stressed regions of the joint. However the results for the X60 material predict lives in the LCF regime in the HAZ at the weld root (point A) for all wave amplitudes, and in the PM adjacent to the weld root (point B) at wave amplitudes above approximately 2.5 m. It can also be seen that the life predictions for the X60 model at wave amplitudes

above 4 m are affected by stress redistribution away from points A, B and C as a result of the elastic shakedown phenomenon, highlighted in Figure 13. A strain based fatigue assessment methodology may be more suitable for life estimation in the X60 material, where yielding has occurred.

Discussion

Bending moment effects

The local axisymmetric girth weld modelling did not account for the effect of the bending moment loading on the SCR. It was determined that for the global SCR models analysed, the additional stress as a result of the bending moment, as shown in Figure 15, is almost negligible in comparison to the axial and hoop stress loading on the SCR.

The predicted bending stress contribution was calculated based on the results shown in Figure 9 using the bending equation. The maximum additional contribution to the direct axial stress by the bending moment would be less than 8% of the nominal axial stress, even at a high wave amplitudes.

Future work

Future work on the global modelling of SCRs will focus on the possible effects of different riser configurations, and metocean data from an offshore production location will be used to obtain a more realistic distribution of the loading expected for a SCR over its lifetime. The effect of more complex SCR-seabed interactions on the loading experienced particularly in the touchdown zone and sag bend of the SCR will also be considered. Future work on the detailed local modelling of SCR girth welds will use a submodelling approach. Using this methodology the stress boundary conditions obtained during the global Flexcom analysis for a region of interest on the SCR can be applied to a 3D full revolution model of an SCR girth weld in Abaqus. This 3D model

may then supply the boundary conditions for a more detailed model of a region of interest on the girth weld through nodal displacements. The authors also intend to include J_2 plasticity constitutive behaviour for each of the weld regions, and to predict damage accumulation in the local model through the use of a UMAT user subroutine in Abaqus.

Conclusions

Global dynamic analysis was conducted using Flexcom on two different SCR models over a wide range of wave amplitudes. The results of the global analysis predicted that the hang-off zone of the SCR was the critical region for both models; this is a region known for its susceptibility to fatigue failure.

Axial stress was the dominant component of mean and alternating stress at this fatigue hot spot. The additional effect of bending moment loading in this region was shown to be negligible in comparison to the contributions of the other loading modes, therefore allowing local axisymmetric modelling of the detailed girth weld geometries for analysis in Abaqus.

The results of the local analyses revealed the importance of control over the weld root geometry. Plasticity was predicted in the HAZ at this location on the inner surface of the SCR for both the 15 mm and 25 mm WT girth weld geometries. The X60 material was found to be susceptible to weld root plasticity in the HAZ for both of the local girth weld geometries analysed, whereas X100 was shown to be susceptible to yielding in the HAZ at the weld root only for the 15 mm WT case. The geometrical attributes of the girth weld were shown to be important, concomitantly with the inhomogeneity in material properties caused by the welding process.

The effect of cyclic loading on the stress distribution in the local girth weld models was determined by observing the cyclic axial stress at an 8 m wave amplitude,

at a location in the HAZ of the 25 mm WT model with X60 material properties. The maximum levels of axial stress and axial stress range were observed within the initial loading cycles, before reducing to a constant level within 6 cycles due to stress redistribution within the weld and the elastic shakedown phenomenon. This has been primarily attributed to the assumption of cyclic load control.

The results of the fatigue analysis conducted on the 25 mm WT girth weld model show the superior performance of the X100 material. Under normal operating conditions the PM, WM and HAZ of the 25 mm WT model would be expected to demonstrate a fatigue life in the HCF regime, which is the desired range for SCR design. The results for the X60 material predict markedly lower lives than X100 for the PM, WM and HAZ at low wave amplitudes, but are affected by stress redistribution in the weld for higher wave amplitudes.

For both the 15 mm and 25 mm WT local girth weld models with X60 and X100 material properties, the HAZ at the weld root on the inner surface of the SCR is found to be the critical location. Yielding is predicted at this location for all analyses using X60 material properties, and in the 15 mm WT model using X100 properties also. For both X100 and X60, the lowest fatigue lives are also predicted in the HAZ at the weld root.

References

Abelanet, M., Karunakaran, D., Jones, R., Eyssautier, S., & White, P. (2013, October). Deepwater steel catenary risers require attention to fatigue factors. *Offshore Magazine*.

API Specification 5L, & ISO 3183. (2008). *Specification for Line Pipe* (Vol. 44th editi).

Beyer, J., Trannum, H. C., Bakke, T., Hodson, P. V., & Collier, T. K. (2016). Environmental effects of the Deepwater Horizon oil spill: A review. *Marine*

Pollution Bulletin, *110*(1), 28–51. http://doi.org/10.1016/j.marpolbul.2016.06.027

Cahoon, J. R. (1972). An improved equation relating hardness to ultimate strength. *Metallurgical Transactions*, *3*(11), 3040. http://doi.org/10.1007/BF02652880

Chibueze, N. O., Ossia, C. V., & Okoli, J. U. (2016). On the Fatigue of Steel Catenary Risers. *Strojniški Vestnik - Journal of Mechanical Engineering*, *62*(12), 751–756. http://doi.org/10.5545/sv-jme.2015.3060

Del Llano-Vizcaya, L., Rubio-González, C., Mesmacque, G., & Cervantes-Hernández, T. (2006). Multiaxial fatigue and failure analysis of helical compression springs. *Engineering Failure Analysis*, *13*(8), 1303–1313. http://doi.org/10.1016/j.engfailanal.2005.10.011

Farragher, T. P., Scully, S., O'Dowd, N. P., Hyde, C. J., & Leen, S. B. (2014). High Temperature, Low Cycle Fatigue Characterization of P91 Weld and Heat Affected Zone Material. *Journal of Pressure Vessel Technology*, *136*(2), 21403. http://doi.org/10.1115/1.4025943

Flexcom Version 8.4.1 Examples Manual. (2015). Galway: Wood Group Kenny.

Flexcom Version 8.4.1 Software Documentation. (2015). Galway: Wood Group Kenny.

Hu, G., Campbell, M., & Huang, C. (2014). Dynamic Plastic Deformation of Deepwater Steel Catenary Risers Under Extreme Cyclic Compressive Loading. In *Offshore Technology Conference* (pp. 73–79). Houston.

Ishikawa, N., Okatsu, M., Endo, S., Kondo, J., Zhou, J., & Taylor, D. (2008). Mass Production and Installation of X100 Linepipe for Strain-based Design Application. *7th International Pipeline Conference*, 1–7. http://doi.org/10.1115/IPC2008-64506

Kopp, F., Perkins, G., Prentice, G., & Stevens, D. (2003). Production and Inspection Issues for Steel Catenary Riser Welds. In *Offshore Technology Conference* (pp. 1–14). Offshore Technology Conference. http://doi.org/10.4043/15144-MS

Lemaitre, J., & Desmorat, R. (2005). *Engineering Damage Mechanics*. Berlin.

Li, M., Barrett, R. A., Scully, S., Harrison, N. M., Leen, S. B., & O'Donoghue, P. E. (2016). Cyclic plasticity of welded P91 material for simple and complex power plant connections. *International Journal of Fatigue*, *87*, 391–404. http://doi.org/10.1016/j.ijfatigue.2016.02.005

Maddox, S. J., Speck, J. B., Razmjoo, G. R., & Park, G. (2008). An Investigation of the Fatigue Performance of Riser Girth Welds. *Journal of Offshore Mechanics and Arctic Engineering*, *130*(February), 1–11. http://doi.org/10.1115/1.2827956

Manning, M. (2016). Today in Energy - Offshore oil production in deepwater and ultra-deepwater is increasing. *U.S. Energy Information Administration (EIA)*. Retrieved from http://www.eia.gov/todayinenergy/detail.php?id=28552

Manson, S. S. (1965). *Fatigue: A complex subject - some simple approximations*. Cleveland.

Mecozzi, E., Lecca, M., Sorrentino, S., Large, M., Davies, C., Gouveia, H., … Perdikaris, P. (2010). *EUR 24214 - Fatigue behaviour of high-strength steel-welded joints in offshore and marine systems (FATHOMS)*. Luxembourg.

Netto, T. A., Botto, A., & Lourenco, M. I. (2008). Fatigue performance of pre-strained pipes with girth weld defects: Local deformation mechanisms under bending. *International Journal of Fatigue*, *30*(6), 1080–1091. http://doi.org/10.1016/j.ijfatigue.2007.08.001

O'Brien, P. J., McNamara, J. F., & Grealish, F. (1991). Extreme Bending and Torsional Responses of Flexible Pipelines. In *Proeedings of the 11th International Offshore Mechanics and Arctic Engineering Symposium* (pp. 319–324). Calgary: ASME.

Saglar, N., Toleman, B., & Thethi, R. (2015). Frontier Deepwater Developments - The Impact on Riser Systems Design in Water Depths Greater than 3,000m. In

Offshore Technology Conference (pp. 1–22). Houston: Offshore Technology Conference. http://doi.org/10.4043/25840-MS

Sweeney, C. A., McHugh, P. E., McGarry, J. P., & Leen, S. B. (2012). Micromechanical methodology for fatigue in cardiovascular stents. *International Journal of Fatigue*, *44*, 202–216. http://doi.org/10.1016/j.ijfatigue.2012.04.022

Vidic-Perunovic, J., Guo, X. S., Wang, L., Hopen, F., & Head, W. J. (2014). Steel Catenary Riser Design for Cylindrical FPSO Application in Ultra-Deep GoM. In *Offshore Technology Conference*. Offshore Technology Conference. http://doi.org/10.4043/25406-MS

Wirsching, P. H. (1984). Fatigue Reliability for Offshore Structures. *Journal of Structural Engineering*, *110*(10), 2340–2356. http://doi.org/10.1061/(ASCE)0733-9445(1984)110:10(2340)

Zhang, X. P., & Dorn, L. (1998). Estimation of the local mechanical properties of pipeline steels and welded joints by use of the microshear test method. *International Journal of Pressure Vessels and Piping*, *75*, 37–42.

Table 1. Material properties and profiles of the global SCR models analysed.

Model	*E* (GPa)	*v*	*OD* (mm)	*WT* (mm)
1	200	0.3	406.4	25
2	200	0.3	406.4	15

Table 2. The constitutive material properties used during local girth weld and fatigue analyses.

	X60			*X100*		
	PM	*WM*	*HAZ*	*PM*	*WM*	*HAZ*
E (GPa)	199.69	202.4	195.85	199.69	202.4	195.85
v	0.3	0.3	0.3	0.3	0.3	0.3
σ_y (MPa)	500.2	500.1	440.1	719.5	826.5	681
σ_{TS} (MPa)	556.53	576.88	504.5365	828.5	888.5	778
σ_f' (MPa)	1057.41	1096.07	958.62	1574.15	1688.15	1478.2
b	-0.12	-0.12	-0.12	-0.12	-0.12	-0.12
n	-	-	-	-	-	0.058

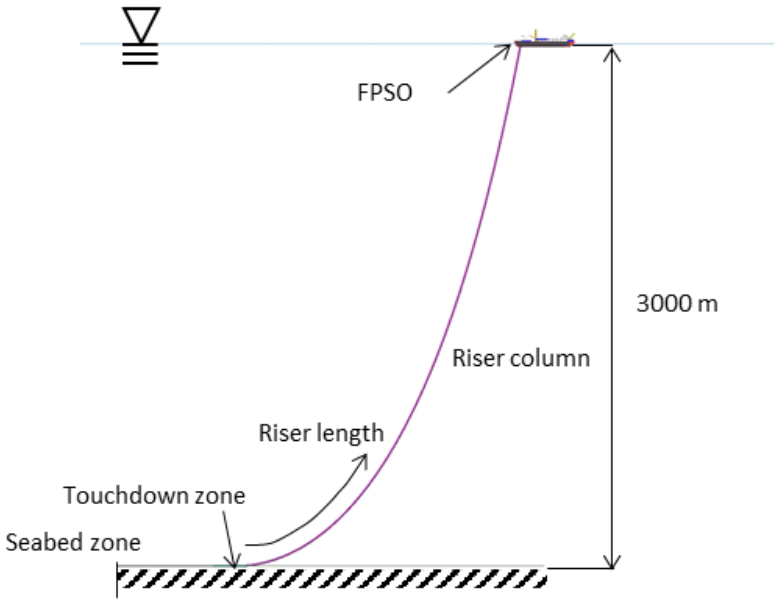

Figure 1. A schematic image of the global SCR model used during Flexcom analysis. The three zones of mesh refinement are labelled and highlighted.

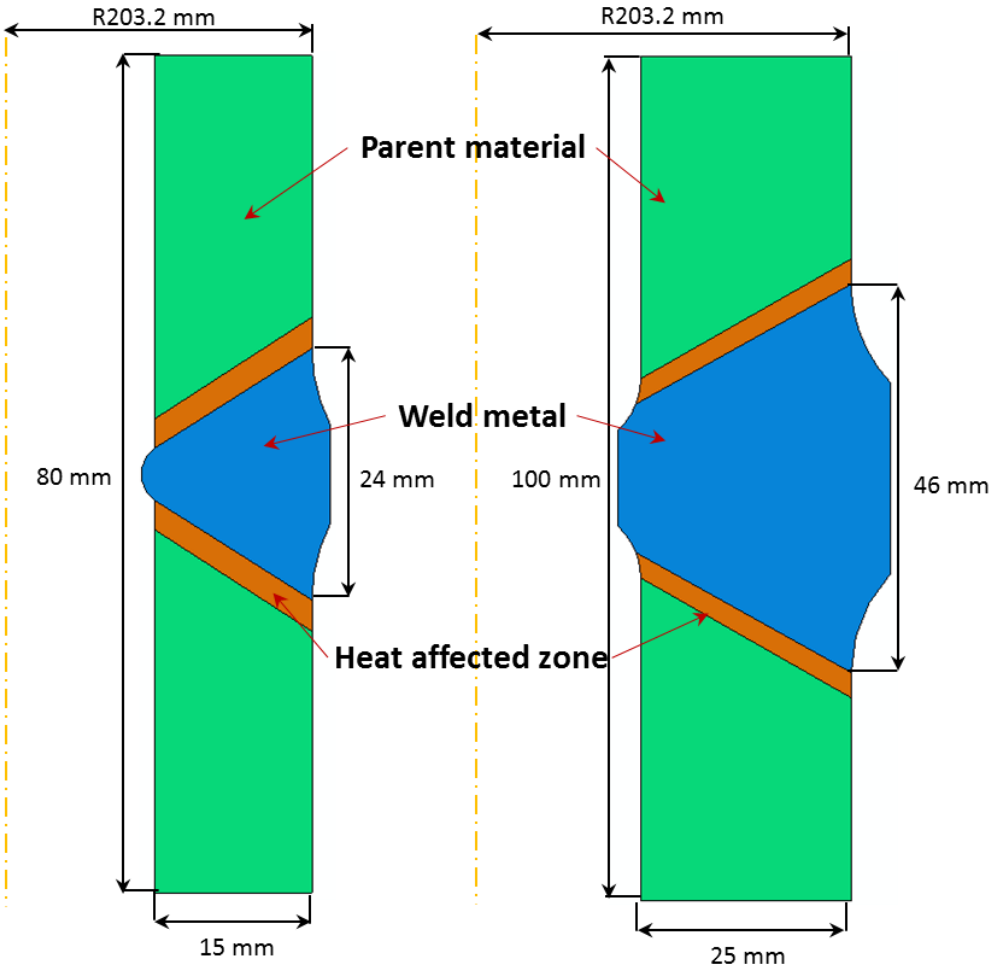

Figure 2. A dimensioned schematic image of the 15 mm and 25 mm WT girth weld models (All dimensions in mm).

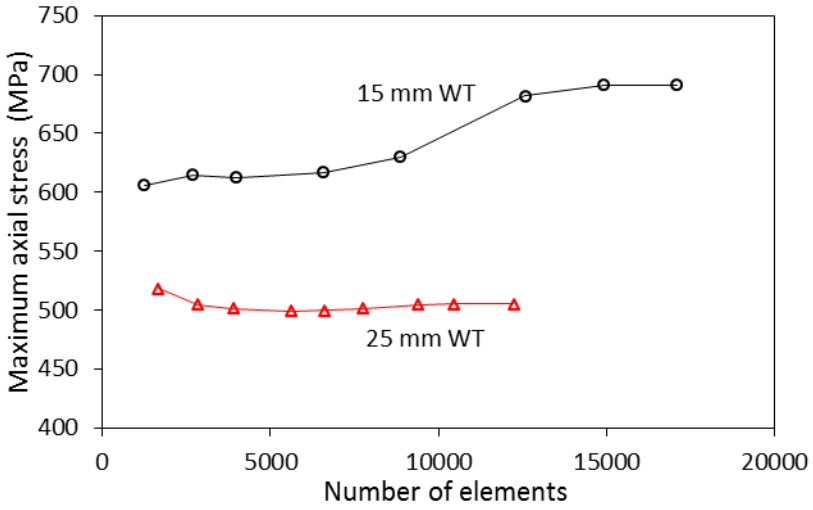

Figure 3. Results of the convergence study, conducted at a 2 m wave amplitude on X60 material.

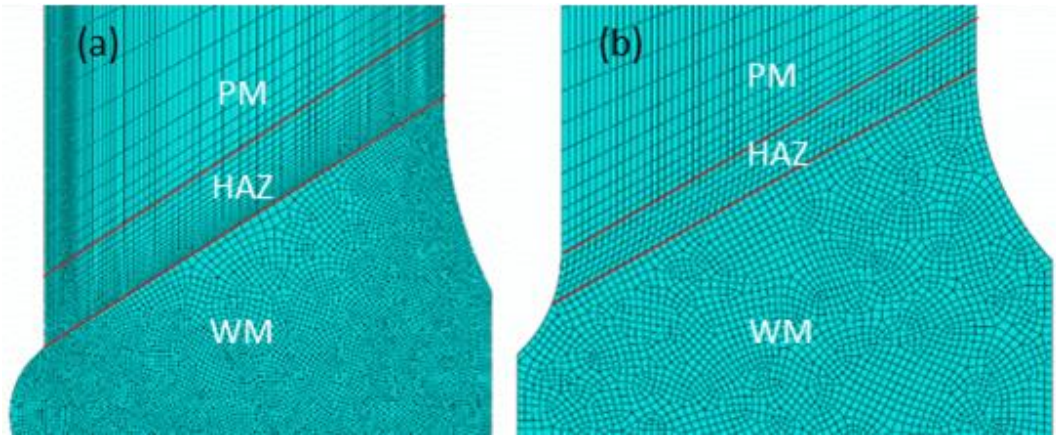

Figure 4. Detail view of the converged mesh for the (a) 15 mm WT model and (b) 25 mm WT model.

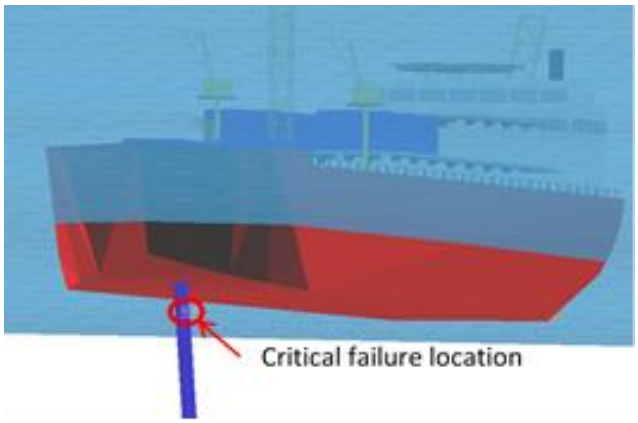

Figure 5. The critical failure location in the hang off zone which was determined during global analyses.

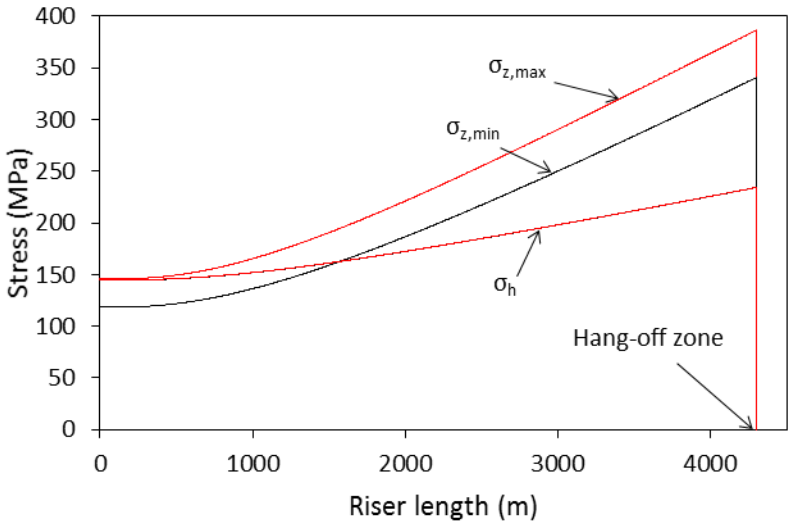

Figure 6. The envelopes of axial (σ_z) and hoop (σ_h) stress along the SCR length for the 15 mm WT model at a wave amplitude of 2 m.

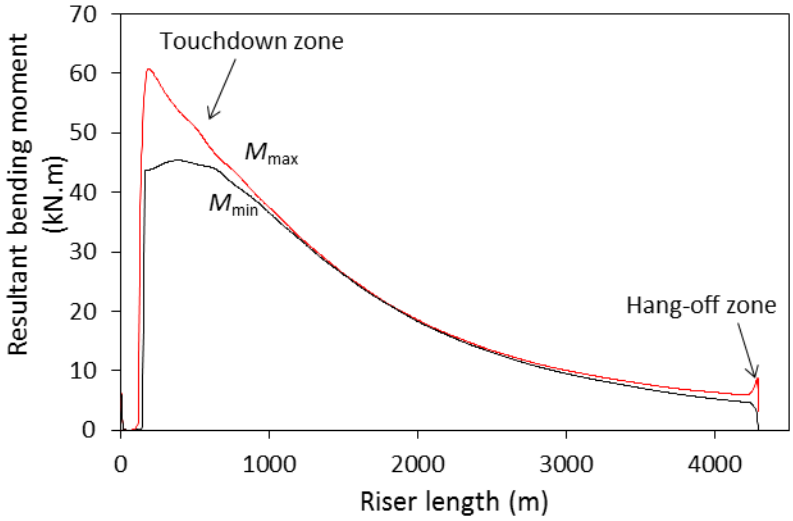

Figure 7. The envelope of resultant bending moment along the length of the SCR for the 15 mm WT model at a wave amplitude of 2 m.

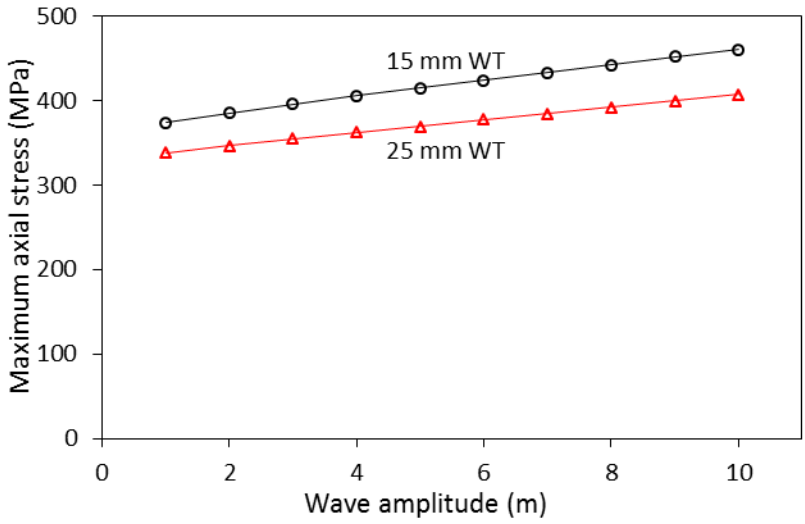

Figure 8. Plot of the maximum axial stress predicted at the failure critical element during global analyses.

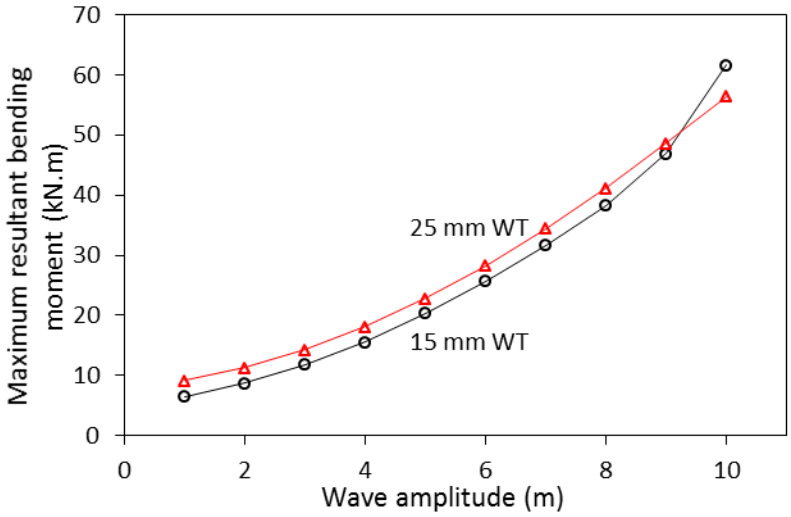

Figure 9. Plot of the maximum bending moment predicted at the failure critical element during global analyses.

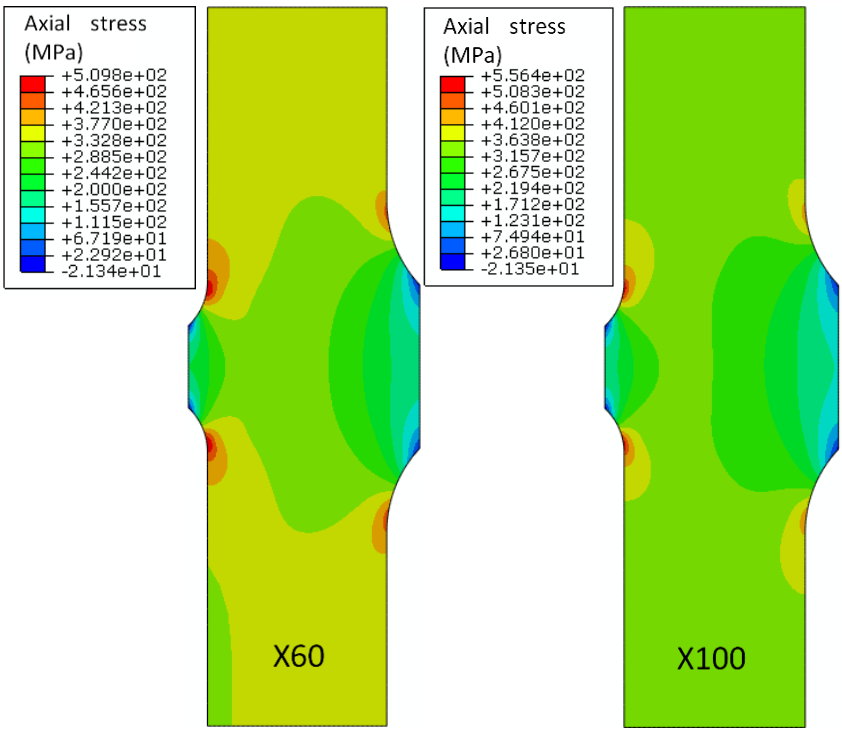

Figure 10. Contour plots of the maximum axial stress distribution at a 2 m wave amplitude on the 25 mm WT model.

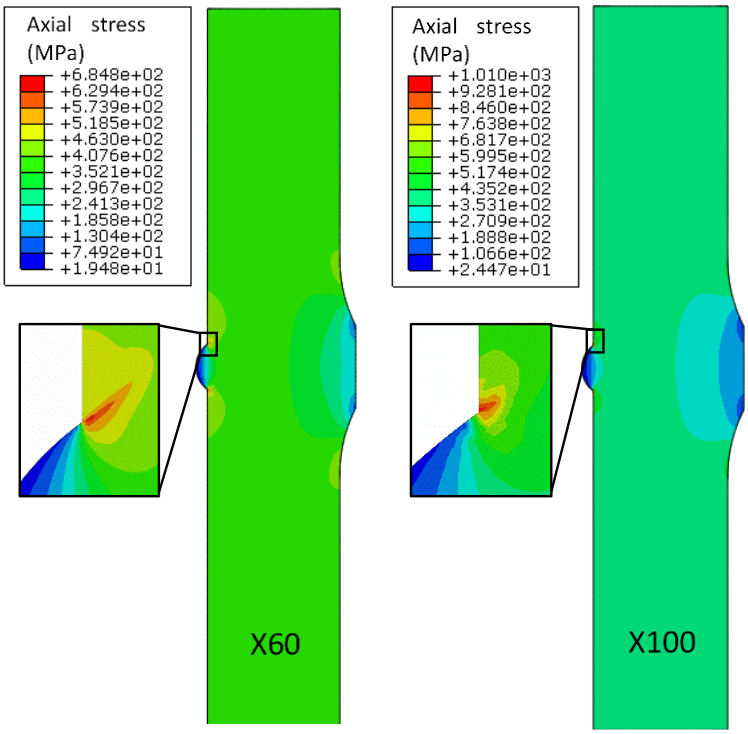

Figure 11. Contour plots of the maximum axial stress distribution for a 2 m wave amplitude on the 15 mm WT model.

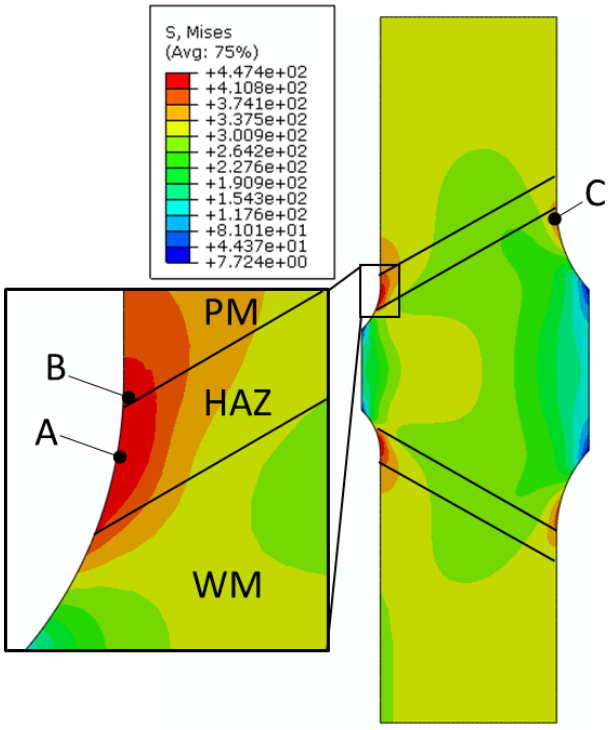

Figure 12. Contour plot of the maximum cyclic von Mises stress on the 25 mm WT X60 girth weld model at a 2 m wave amplitude, highlighting points A (HAZ), B (PM).and C (WM).

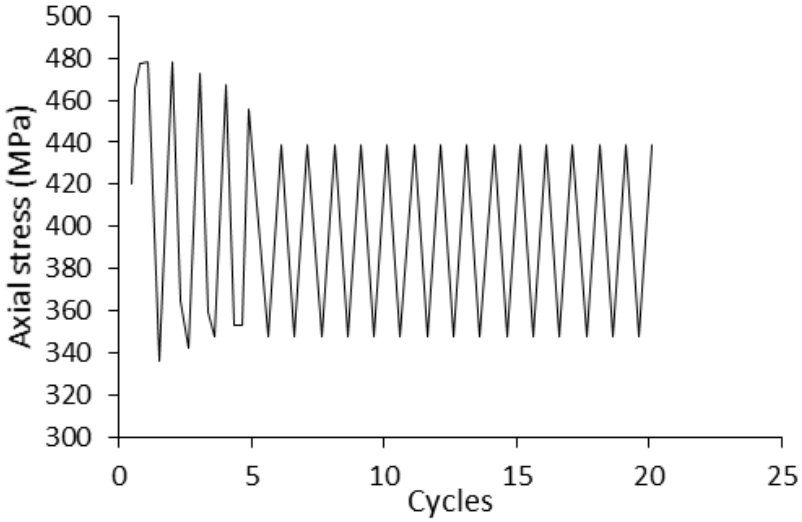

Figure 13. Plot of the axial stress response over 20 cycles for the hot spot located at point A in the HAZ at the weld root, for the 25 mm WT X60 model at an 8 m wave amplitude.

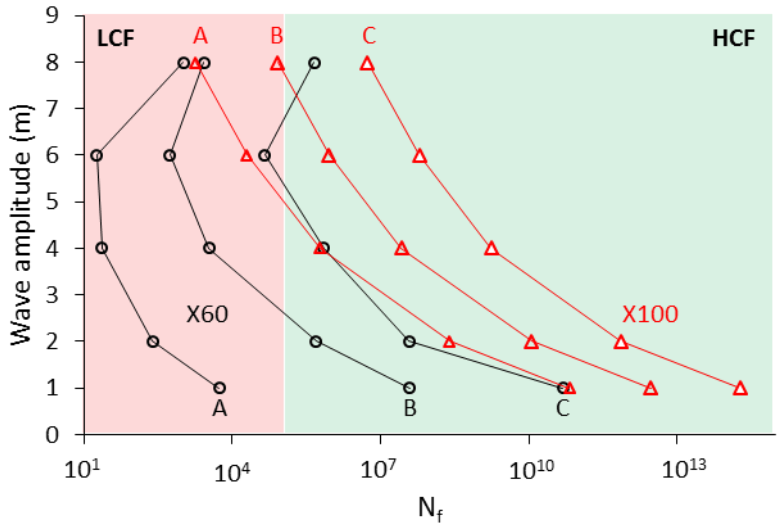

Figure 14. Plot of the lives predicted using the combined Goodman-Basquin equation at locations A (HAZ),B (PM) and C (WM) for both the X60 and X100 25 mm WT model for a range of wave amplitudes.

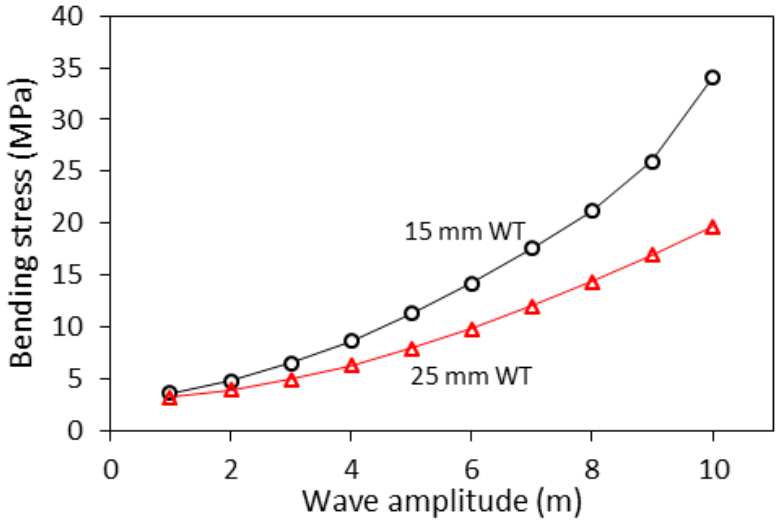

Figure 15. Plot of bending stress calculated at the critical region, based on the results shown in Figure 9.